HHS Public Access

Author manuscript

Cancer Res. Author manuscript; available in PMC 2022 February 01.

Published in final edited form as:

Cancer Res. 2021 August 01; 81(15): 4145–4154. doi:10.1158/0008-5472.CAN-20-3822.

Transient competitive inhibition bypasses the binding site barrier to improve tumor penetration of trastuzumab and enhance T-DM1 efficacy

Brandon M. Bordeau[1], **Yujie Yang**[1], **Joseph P. Balthasar**[1]

[1] Department of Pharmaceutical Science, University at Buffalo, Buffalo, NY 14214

Abstract

Poor penetration of monoclonal antibodies (mAb) in solid tumors is explained in part by the binding site barrier hypothesis. Following extravasation, mAbs rapidly bind cellular antigens, leading to the observation that, at sub-saturating doses, therapeutic antibody in solid tumors localizes around tumor vasculature. Here we report a unique strategy to overcome the binding site barrier through transient competitive inhibition of antibody-antigen binding. The anti-trastuzumab single domain antibody 1HE was identified through in vitro binding assays as a model inhibitor. Co-administration of 1HE did not alter the plasma pharmacokinetics of trastuzumab or ado-trastuzumab emtansine (T-DM1) in vivo. Administration of 1HE alone was rapidly eliminated with a terminal plasma half-life of 1.2 hours, while co-administrations of 1HE with trastuzumab had a terminal half-life of 56 hours. In mice harboring SKOV3 xenografts, co-administration of 1HE with trastuzumab led to significant increases in both penetration of trastuzumab from vasculature and the percent of tumor area that stained positive for trastuzumab. 1HE co-administered with a single dose of T-DM1 to NCI-N87 xenograft bearing mice significantly enhanced T-DM1 efficacy, increasing median survival. These results support the hypothesis that transient competitive inhibition can improve therapeutic antibody distribution in solid tumors and enhance antibody efficacy.

Keywords

Trastuzumab; T-DM1; Antibody distribution; Binding site barrier; Competitive Inhibition

INTRODUCTION

Interest in the development of targeted anti-cancer therapeutics such as monoclonal antibodies (mAbs) and antibody-cytotoxin conjugates has grown rapidly over the past two decades. In total, 30 antibodies have received Food and Drug Administration (FDA) approval for oncology indications with 6 currently in regulatory review and an additional 40 in late-stage clinical development (1). However, it is recognized that antibodies often exhibit only limited uptake and penetration in solid tumors, leading to suboptimal efficacy (2–4).

Corresponding author: Joseph P. Balthasar, jb@buffalo.edu, 450 Kapoor Hall, Buffalo, NY, USA 14214, T: 716-645-4807.

Solid tumors are responsible for ~90% of the total deaths from cancer (5) and, consequently, methods to improve antibody efficacy against solid tumors may have great clinical impact.

Physical barriers present within solid tumors are well appreciated in impeding uptake and penetration of therapeutic antibodies. Poor distribution of mAbs within tumors has been attributed to many factors (2,3,6), and improved intratumoral distribution has been achieved with tumor matrix modulation (7–9) and vascular permeability enhancement (10–12). An impediment to antibody penetration that remains a significant challenge is the binding site barrier (BSB) (13–15). The tumor penetration of high-affinity antibodies is limited by the successful binding of antibodies to cellular antigens at the point of extravasation, leading to antibody sequestration and sub-optimal tumor exposure (14,16–18). The BSB was first described more than 30 years ago (19); subsequently, a large number of experimental investigations and mathematical simulations have supported the BSB hypothesis (14–18,20). Preclinical investigations have shown increased intra-tumoral distribution for low or intermediate affinity mAb and lower molecular weight constructs (e.g., sdAb, scFv, Fab) (14,17,18,21–25); however, clinical utility has not yet been established. The vast majority of anti-cancer antibody therapies on the market and in development are high-affinity, intact mAb, where distribution within solid tumors is often strongly impacted by the binding site barrier phenomenon.

Recently, there has been substantial discussion of the impact of the BSB on the efficacy of antibody-drug conjugates (ADC) (26–30). Due to dose limiting toxicities, ADCs are administered at doses below levels required to saturate antigen throughout the tumor. Under these non-saturating conditions, the impact of the BSB is most evident, and promotes substantial heterogeneity in antibody concentrations throughout tumors, with high concentrations near sites of extravasation, and with dramatically reducing ADC concentrations with increasing distance from tumor blood vessels. Due to the high potency of ADC, concentrations in excess of those required for cell killing are achieved near vessels, and concentrations far below those required for efficacy are found at locations distant from sites of extravasation (28). Consequently, at clinical ADC doses, the BSB results in excess delivery of ADC to tumor cells surrounding vasculature at the expense of poor total tumor exposure to ADC (28).

Here we report a strategy to overcome the BSB through transient competitive inhibition of mAb-antigen binding. We hypothesized that transient competitive inhibition of antibody binding to tumor antigens would increase the distribution of mAb within solid tumors, retaining the high tumor selectivity of a high-affinity mAb, while enabling the desirable within-tumor distribution characteristics of a low-affinity mAb (illustrated graphically in Figure 1A and 1B). The anti-idiotypic anti-trastuzumab camelid single-domain antibody (sdAb), 1HE, reported by Alvarez-Reuda et al. for the development of a human epidermal growth factor receptor 2 (HER2) vaccine (31), was identified using in-vitro binding assays as a lead inhibitor for experimental evaluation of the competitive inhibition strategy. 1HE coadministration did not alter the plasma pharmacokinetics of trastuzumab or T-DM1 in Swiss-Webster mice. When administered alone, 1HE was rapidly eliminated from plasma. However, when administered with trastuzumab, 1HE elimination was dramatically reduced, consistent with 1HE bound to trastuzumab being protected from kidney filtration and

catabolism. In mouse xenograft models of HER2 positive carcinoma, 1HE co-administration significantly increased trastuzumab penetration within tumors and improved T-DM1 efficacy. Results that are provided here indicate that transient inhibition of HER2 binding allows trastuzumab to bypass the binding site barrier, without losing the benefit of high-affinity HER2 binding. The competitive inhibition strategy, which may be applied to a wide range of high-affinity anti-cancer antibody therapies that are on the market and in current development, may be a clinically feasible approach to enhance the effectiveness of targeted therapies directed against solid tumors.

MATERIALS AND METHODS

Materials

The human ovarian carcinoma cell-line SKOV3 (HTB-77, RRID:CVCL_0532) was purchased from American type culture collection (ATCC, Manassas, VA) and the gastric carcinoma cell line NCI-N87 (CRL-5822, RRID:CVCL_WH01) was a generous gift from Dr. Dhaval Shah. Cell-lines were authenticated by ATCC using short tandem repeat profiling and were tested for mycoplasma contamination using a universal mycoplasma detection kit (ATCC® 30–1012K™) in January of 2021. Cells were cultured following ATCC cell-line specific recommendations and were used within the first 10-passages following thawing. Trastuzumab and ado-trastuzumab emtansine were purchased from Millard Fillmore Memorial Hospital (Amherst, NY).

1HE expression and purification

The amino acid sequence for 1HE was obtained from the publication by Alvarez-Reuda et al. (31). A codon-optimized 1HE DNA sequence was synthesized by GeneArt, ligated into the plasmid pET22b(+) (Millipore-Sigma, Burlington, MA, 69744) at the XhoI and NdeI restriction enzyme sites, and transformed into the *E. coli* strain SHuffle (New England Biolabs, Ipswich, MA, C3029J). 1HE was produced in SHuffle cells following a standard recombinant expression protocol. Briefly, a glycerol stock of transformed SHuffle cells was removed from storage at −80 °C and a small volume spread over a lysogeny broth (LB) agar plate with 100 μg/ml ampicillin. The next day a single colony was selected and inoculated into an LB medium starter culture with 100 μg/ml ampicillin and grown in a shaker incubator at 30 °C for 18 hours. The starter culture was diluted 1 to 100 into LB medium with 100 μg/ml ampicillin and cells grown to an optical density of 0.6–0.8 at a wavelength of 600 nm and expression induced with 1 mm isopropyl β-d-1-thiogalactopyranoside (IPTG) for 18 hours at 16 °C. Cells were pelleted, lysed using BugBuster® (Millipore-Sigma, Burlington, MA, 70584), and 1HE purified from cell lysate with a 3 mL HisPur™ Ni-NTA spin column (Thermo Fisher Scientific, Waltham, MA, 88226) following manufacturer recommendations. Eluted protein was dialyzed into a 5 mM disodium phosphate buffer pH 6.8 overnight and the dialyzed product flowed through a Bioscale Mini-CHT Type 1 cartridge (BioRad, Hercules, CA, 7324324) using a BioLogic LP system (BioRad, Hercules, CA). 1HE was eluted from the CHT column using a 100 mL gradient of 0–100% 500 mM disodium phosphate at a flow rate of 2 mL/minute. Collected fractions were analyzed with sodium dodecyl sulfate–polyacrylamide gel electrophoresis (SDS-PAGE) and fractions

containing 1HE combined and dialyzed into phosphate-buffered saline pH 7.4 (PBS) overnight.

Surface plasmon resonance (SPR)

A SR7500DC SPR (Reichert, Depew, NY) was utilized for kinetic binding assessment. Trastuzumab was immobilized on a CM5 chip (Reichert, Depew, NY, Part #: 13206066) through amine coupling. For all binding assessments, a mobile phase of 0.05% Tween-20 PBS pH 7.4 was used at a flow rate of 25 μL/minute. Binding kinetics for 1HE to trastuzumab was evaluated through injection of 1HE at concentrations of 1, 3, 7.5, 15, and 30 nM for 2.5 minutes with a 10-minute dissociation. A second evaluation of 1HE-trastuzumab binding was completed with a 10-hour dissociation time with 1HE injections at concentrations of 10, 20, and 35 nM. Association and dissociation rate constants were determined using a 1:1 Langmuir binding model in the biosensor data analysis software Scrubber (BioLogic Software, Canberra, Australia).

Radiolabeling of trastuzumab and 1HE

Trastuzumab, T-DM1, and 1HE were radiolabeled with iodine-125 (^{125}I) through a modified chloramine-T method described previously (32). Briefly, 40 μL of protein (1–2 mg/mL in pH 7.4 PBS) was combined with 10 μL of sodium^{125}I (100 mCi/mL) (PerkinElmer, Waltham, MA), and subsequently reacted with 20 μL of chloramine-T (1 mg/mL in pH 7.4 PBS). After 90 seconds, the reaction was terminated by the addition of 40 μL of 10 mg/mL potassium iodide. Immediately following the reaction, gel filtration (Sephadex G-25 column, GE Healthcare Bio-Sciences, Pittsburgh, PA) was performed to separate ^{125}I labeled intact mAb from the mixture. The activity of the ^{125}I-protein fraction was determined through gamma counting (LKB Wallac 1272, Wallac, Turku, Finland) with purity assessed through thin layer chromatography (PE SiL-G, Whatman Ltd, Kent, England).

Assessment of 1HE inhibition on ^{125}I-trastuzumab-HER2 binding

SKOV3 cells (ATCC, HTB-77) were grown in complete McCoy's 5a media to confluency in a T75 flask and dissociated using 50 μM ethylenediaminetetraacetic acid (EDTA). Cells were pelleted (200 RCF, 5 minutes) and resuspended in a 1% bovine serum albumin (BSA) PBS solution and pipetted into microcentrifuge tubes (1 million cells/mL). ^{125}I-trastuzumab was added to each tube, at a concentration of 200 pM, with increasing concentrations of 1HE. Cells were incubated at 4 °C for 90 minutes to reach binding equilibrium followed by 4 washes with 1 mL of 1% BSA PBS buffer to remove non-specific radioactivity. Cell-associated radioactivity was assessed through gamma counting. Cell-associated radioactivity normalized to a ^{125}I-trastuzumab control (B/Bo) was fit to a 3-parameter logistic function in Graphpad Prism 7 (GraphPad, San Diego, CA).

Determination of ^{125}I-1HE dissociation from immobilized trastuzumab

Trastuzumab was chemically conjugated to Dynabeads following manufacturer recommendations (Thermo Fisher Scientific, Waltham, MA, 14321D). ^{125}I-1HE was incubated with trastuzumab beads for 1 hour at a concentration of 10 nM; subsequently, beads were washed 3x with 0.1% BSA-PBS and initial bound radioactivity determined

through gamma-counting. ^{125}I-1HE bound trastuzumab beads were incubated in triplicate with 0.1% BSA-PBS, 1 μM unlabeled 1HE in 0.1% BSA-PBS, or 1 μM T-DM1 in 0.1% BSA-PBS. The supernatant was removed and replaced with fresh buffer at 0.5, 1, 3, 6, 10, 18, 26, 43, and 66 hours, and remaining bound radioactivity determined at each time point.

Impact of 1HE on trastuzumab and T-DM1 plasma pharmacokinetics

Plasma pharmacokinetics of trastuzumab and T-DM1 with and without co-administration of 1HE were assessed in male Swiss-Webster mice 4–6 weeks of age (Envigo, Indianapolis, IN). Mouse studies were approved by the University at Buffalo Institutional Animal Care and Use Committee. Trastuzumab was given through penile vein injection at doses of 0.1, 1, and 10 mg/kg (5 mice/group) with and without 1HE in a 1:2 molar ratio (trastuzumab:1HE) with a tracer dose of ^{125}I-trastuzumab (400 μCi/kg). T-DM1 was administered at a dose of 1.8 mg/kg with a tracer dose of ^{125}I-T-DM1 (400 μCi/kg). 1HE was administered at a 10-fold molar excess through retro-orbital injection 15 minutes after T-DM1 injection with T-DM1 only control mice receiving a volume equivalent of PBS. Blood samples were collected through retro-orbital sampling using microcapillary tubes coated with ethylenediaminetetraacetic acid (EDTA). Plasma samples were collected following centrifugation (200 xg, 5 minutes), and trichloroacetic acid (TCA) precipitated as previously described (33). Plasma associated radioactivity was determined through gamma-counting (LKB Wallac 1272, Wallac, Turku, Finland) with observed counts corrected for background radiation and radioactive decay. Noncompartmental analysis (WinNonlin 7, Phoenix, Pharsight Corporation, Palo Alto, CA) was used for calculation of the area under the curve from 0–10 days after administration ($AUC_{(0–10days)}$). The observed $AUC_{(0–10days)}$ with and without 1HE co-administration was compared statistically using Student's t-test with Bonferroni's correction for multiple comparisons in GraphPad Prism 7 (GraphPad, San Diego, CA).

1HE plasma pharmacokinetics

1HE pharmacokinetics were assessed following a 1 mg/kg dose in male Swiss-Webster mice 4–6 weeks of age (Envigo, Indianapolis, IN). Blood samples were collected at 5, 20, 60, 180, and 360 minutes after injection through retro-orbital or submandibular sampling and plasma samples collected following centrifugation (200 rotational centrifugal force (RCF), 5 minutes). 1HE timepoints were quantified using the indirect ELISA protocol provided in the supplementary information. ELISA variability and recovery values are provided in supplementary table 1. 1HE plasma pharmacokinetics with trastuzumab was evaluated at a trastuzumab to 1HE ratio of 1: 0.2 with a ^{125}I-1HE (400 μCi/kg) tracer dose. Of note, the ratio of 1:0.2 trastuzumab to unlabeled 1HE was used to ensure the availability of free trastuzumab sites for binding to ^{125}I-1HE. Blood samples were collected through retro-orbital sampling using microcapillary tubes coated with EDTA. Plasma samples were collected following centrifugation (200 RCF, 5 minutes), and TCA precipitated. Following TCA-precipitation plasma associated radioactivity was determined through gamma-counting with observed counts corrected for background radiation and radioactive decay.

Assessment of trastuzumab penetration in SKOV3 xenografts

Male NOD-SCID mice (Charles-River, Wilmington, MA) were subcutaneously injected with two million SKOV3 cells in DPBS in the right flank. Once tumors reached an average size of 200 mm^3 the mice were intravenously injected with 2 mg/kg trastuzumab alone or with 1HE in a 1:2 molar ratio (trastuzumab:1HE) (n=3/group). 24-hours after intravenous injection the xenografts were resected, cryosectioned, and trastuzumab and tumor vasculature fluorescently stained. The complete staining protocol is provided in the supplementary information. Tumor sections were imaged using an EVOS Fl autofluorescent microscope (Thermo Fisher Scientific, Waltham, MA) using an identical automated imaging method for each slice. Three tumor sections per tumor were analyzed to obtain trastuzumab penetration values using an image analysis protocol and algorithm that is described and provided in the supplementary information.

T-DM1 efficacy

Male NU/J mice, 4–6 weeks (The Jackson Laboratory, Bar Harbor, ME), were injected subcutaneously in the right flank with 5 million NCI-N87 cells in 200 μl of a 1:1 matrigel (Thermo Fisher Scientific, Waltham, MA, CB-40234): RPMI 1640 solution. Tumor size was measured using digital calipers with tumor volume calculated using the formula: tumor volume=0.5*a^2*b, where a is tumor width and b tumor length. Once tumor volumes reached an average of ~250 mm^3 mice were split into 4 groups: saline vehicle (n=7), trastuzumab 10 mg/kg (n=7), T-DM1 1.8 mg/kg (n=9) and T-DM1:1HE 1.8 mg/kg (n=9). Mice were injected through retro-orbital injection with T-DM1 with either 1HE (10-fold molar excess) or saline administered 15 minutes after T-DM1. Tumor volumes were monitored every two days, and mice sacrificed once tumors reached a terminal volume of 1200 mm^3. Kaplan-Meier survival curves were generated in GraphPad Prism 7 and compared using the log-rank test at a significance level of $p \leq 0.008$.

RESULTS

1HE Trastuzumab Binding Assays

The initial SPR assessment for 1HE-trastuzumab binding resulted in a best-fit koff rate of 4.8×10^{-4} sec^{-1}; however, biphasic binding kinetics were observed (Figure 2 top left panel). Biphasic binding kinetics may be the result of heterogeneity within the purified 1HE preparation or heterogenous immobilization of trastuzumab on the SPR chip, leading to partial occlusion of the 1HE binding site on trastuzumab. Gel-based analysis indicated 1HE was >90% pure with only a single peak observed following SEC and HIC runs (figure S1A, S1B), therefore the bi-phasic kinetics were likely the result of heterogenous trastuzumab immobilization. To further characterize 1HE-trastuzumab dissociation kinetics, a secondary SPR evaluation with a 10-hour dissociation time was employed. The resultant data led to a best-fit koff value of 7.2×10^{-6} sec^{-1} (figure 2 bottom left panel). We hypothesize that the initial koff estimate of 4.8×10^{-4} sec^{-1} overpredicts the true dissociation rate because early phases of dissociation are dominated by dissociation of 1HE from partially blocked trastuzumab binding sites. Of note, it is possible that the 10-hour dissociation koff of 7.2×10^{-6} sec^{-1} underpredicts the true dissociation rate constant due to mass-transport limitations and due to rebinding of 1HE and trastuzumab within the SPR assay run. To

further evaluate trastuzumab-1HE binding, a competitive cell-based assay was conducted (Figure 2 top right panel). 1HE led to a concentration-dependent reduction in the amount of trastuzumab bound to cellular HER2, indicating 1HE is a competitive inhibitor of trastuzumab-HER2 binding. The observed half-maximal inhibition constant (IC50) of 124 pM for 1HE was approximately equal to ~50% of the concentration of trastuzumab added (200 pM), consistent with a 1HE-trastuzumab binding KD ≤124 pM. A secondary evaluation of 1HE-trastuzumab dissociation kinetics was performed using ^{125}I-1HE bound to trastuzumab immobilized Dynabeads (figure 2 bottom right panel). To prevent rebinding bound ^{125}I-1HE was dissociated in solutions of either 1 μM T-DM1 or 1 μM unlabeled 1HE, with the percent radioactivity over time fit to a monophasic decline function. Similar rate constants were observed between the T-DM1 and 1HE groups with koff rates of 1.6×10^{-5} sec^{-1} and 1.7×10^{-5} sec^{-1}, respectively. Trastuzumab bound ^{125}I-1HE incubated in the control buffer had 62% of the initial bound radioactivity remaining at 66 hours, indicating that dissociated ^{125}I-1HE rebound trastuzumab during the incubations.

Effects of 1HE administration on the plasma pharmacokinetics of trastuzumab and T-DM1

Trastuzumab was administered to non-tumor bearing mice, with and without 1HE, and plasma pharmacokinetics were assessed (Figure 3 left panel). Non-compartmental analysis of the plasma pharmacokinetic time profiles indicated there was no significant difference in the $AUC_{(0–10days)}$ for trastuzumab administered alone or with 1HE at doses of 0.1, 1 and 10 mg/kg (Table 1). The clinically approved antibody-drug conjugate of trastuzumab, T-DM1, was also administered with and without 1HE and plasma pharmacokinetics were assessed. Mild precipitation was observed when 1HE and T-DM1 were combined in a single solution; therefore, 1HE was administered at a 10-fold molar excess to T-DM1, 15-minutes after T-DM1 administration. Although the observed precipitation requires further evaluation, co-administration of 1HE with T-DM1 at a dose of 1.8 mg/kg did not significantly impact T-DM1 plasma pharmacokinetics (Figure 3, Table 1).

Plasma pharmacokinetics of 1HE with and without trastuzumab co-administration

1HE administered to Swiss-Webster mice was rapidly eliminated, with less than 5% of the initial plasma concentration remaining 20 minutes after injection and a terminal elimination half-life of 1.2 hours. The 3- and 6-hour time-points were below the lower limit of quantification in plasma (50 ng/mL). Co-administration of 1HE with trastuzumab led to a significant decrease in the elimination of 1HE, with a terminal elimination half-life of 56 hours. The plasma time profile for 1HE alone (1 mg/kg) and 1HE:trastuzumab (0:2:1 ratio) are provided in the right panel of Figure 3. Plasma time profiles are plotted as the fraction of the initial plasma timepoint sample remaining (C/C_0).

Impact of 1HE co-administration on trastuzumab distribution in SKOV3 xenografts

SKOV3 xenografts from mice administered 2 mg/kg trastuzumab alone and with 1HE (1:2 trastuzumab:1HE molar ratio) were fluorescently stained ex-vivo to detect trastuzumab and tumor vasculature. Entire tumor sections were imaged under identical intensities. A representative tumor section from each xenograft bearing mouse that was treated with trastuzumab or trastuzumab:1HE is provided in supplementary figures 2 and 3, respectively. Consistent with previous studies that have assessed trastuzumab tumor distribution at sub-

saturating doses (13), trastuzumab (green) was restricted around vasculature (red) with only a fraction of the total tumor area staining positive for trastuzumab (Figure 4A). Tumor sections obtained from mice administered trastuzumab:1HE demonstrated a more homogeneous staining pattern, with a greater percentage of the tumor area staining positive for trastuzumab (Figure 4B). To enhance visualization of the between-group differences, tumor slices from trastuzumab and trastuzumab:1HE treated mice were converted to black and white images, with black shading applied to regions demonstrating fluorescence exceeding a threshold of two times background (Figures 4C and D). Nine tumor slices from three xenografts were analyzed quantitively per group, with results provided in Table 2. 1HE co-administration significantly increased the percent of the tumor area that stained positive for trastuzumab from 26.52% (standard deviation SD: 8.11%) for trastuzumab alone to 43.32% (SD: 11.42%) for trastuzumab:1HE. The mean fluorescence intensity (MFI) was not significantly different between the groups, whereas the MFI for all pixels two times above background was significantly higher for the trastuzumab only group at 34 MFI (SD: 5) vs. 27 MFI (SD: 3) for trastuzumab:1HE. This observation is consistent with 1HE co-administration leading to an equivalent mass of trastuzumab being spread over a greater area. A MATLAB algorithm was used to obtain the mean distance of all tumor pixels from vasculature (penetration distance limit) and the mean penetration distance of trastuzumab positive pixels from the vasculature. The trastuzumab and trastuzumab:1HE groups had similar penetration limits of 68.60 μm (SD: 15.65) and 64.54 μm (SD: 5.04), respectively. 1HE co-administration significantly increased the penetration distance for trastuzumab associated pixels that had a fluorescence intensity two-times background from 41.30 μm (SD: 6.70) to 58.24 μm (SD: 5.40) and the penetration distance weighted to the pixel fluorescence intensity from 39.38 μm (SD: 5.89) to 51.51 μm (SD: 5.15). Figure 4E shows the fluorescence staining intensity of trastuzumab pixels as a function of distance from the nearest vasculature pixel. The trastuzumab and trastuzumab:1HE groups have similar fluorescence intensities up to 30 μm, whereas, the trastuzumab:1HE tumors have greater fluorescence intensities between 30 μm and 250 μm from the vasculature.

Impact of 1HE co-administration on T-DM1 efficacy in NCI-N87 xenograft bearing mice

T-DM1 is effective when occupying only a fraction of available binding sites on the gastric carcinoma cell line NCI-N87 (34). NCI-N87 xenograft-bearing mice were administered T-DM1 at a dose of 1.8 mg/kg with and without 1HE to assess the impact of 1HE on T-DM1 efficacy. NCI-N87 has been reported to be resistant to trastuzumab monotherapy (34); therefore, trastuzumab was included as an additional control group for model validation. Resulting tumor growth and survival curves are shown in the left and right panels of Figures 5 respectively. Trastuzumab did not significantly extend lifespan in comparison to the control group ($p=0.68$). T-DM1 alone did not significantly improve survival from the saline group ($p=0.033$) or the trastuzumab group ($p=0.27$). T-DM1 co-administered with 1HE had a significant increase in survival from T-DM1 alone ($p=0.005$) and both the trastuzumab ($p=0.004$) and saline groups ($p<0.0001$).

DISCUSSION

Here we describe a strategy to overcome the binding site barrier (BSB) for trastuzumab through competitive inhibition of HER2 binding. The BSB has been implicated as a primary obstacle to therapeutic antibody distribution within solid tumors. Despite the BSB being first characterized in the early 1990s (16,19), this barrier remains a significant challenge. Co-administration of a transient inhibitor of antibody-antigen binding was hypothesized to provide the distributional advantage of an untargeted antibody with the tumor selectivity of a high-affinity antibody. Trastuzumab was chosen as a model antibody for experimental validation of the competitive inhibition strategy. Trastuzumab is widely used for the treatment of breast and gastric cancer, and ado-trastuzumab emtansine and trastuzumab deruxtecan are FDA-approved antibody-drug conjugates. Additionally, trastuzumab has been previously shown to have limited tumor penetration due to high-affinity HER2 binding (13,18). The competitive inhibitor 1HE is a camelid single-domain antibody (VHH) that was reported by Alvarez-Reuda et al., in efforts to generate a HER2 vaccine (31). Using in-vitro binding assays, we identified 1HE as a lead inhibitor for the competitive inhibition strategy. Surface plasmon resonance (SPR) and radio-labeled dissociation studies indicate 1HE bound trastuzumab with a dissociation half-life between 12–27 hours, and that 1HE inhibited trastuzumab binding to cells that overexpress HER2.

Several pharmacokinetic assumptions of our competitive inhibition hypothesis required experimental validations. First, it was assumed trastuzumab's plasma pharmacokinetics are not altered by 1HE. In the early development of the competitive inhibition strategy, our laboratory observed that soluble carcinoembryonic antigen (CEA) increased the elimination of T84.66, leading to a 2-fold decrease in T84.66 tumor exposure (35). This is consistent with the observation that shed mesothelin significantly decreased the efficacy of an anti-mesothelin immunotoxin (36), despite simulations predicting an increase in immunotoxin efficacy with shed antigen due to improved tumor distribution (37). Plasma pharmacokinetic investigations in mice, shown here, indicate trastuzumab and T-DM1 co-administered with 1HE have equivalent plasma pharmacokinetics as the free antibody. The second pharmacokinetic assumption was that the in-vivo dissociation of 1HE from trastuzumab is consistent with the binding kinetics obtained through SPR and radio-labeled dissociation studies. This assumption is critical as a long half-life of inhibition is necessary for trastuzumab to extravasate and diffuse to poorly-vascularized regions prior to 1HE dissociation. If 1HE were to dissociate from trastuzumab faster in-vivo than in-vitro, for example, due to plasma instability of 1HE, then significant enhancements in trastuzumab distribution would not be obtained. The observed terminal half-life of trastuzumab in Swiss-Webster mice was 12.6 days, which is much longer than the binding half-life of 1HE to trastuzumab (between 12 and 27 h, based on in vitro binding assays). 1HE administered with trastuzumab had a terminal half-life of 57 hours, far greater than the half-life of 1HE administered alone. The observed terminal plasma half-life of 1HE administered with trastuzumab exceeds the binding dissociation half-life due to the rebinding of 1HE and trastuzumab in vivo.

Fluorescence microscopy is one of the most common techniques used for the evaluation of antibody distribution in tumors (13,15,17,34). A limitation of fluorescence microscopy is the

potential for bias resulting from manual selection of tumor regions. Several studies have limited user bias through imaging of entire tumor slices and/or quantitative image analysis. Rhoden et al. developed a MATLAB program that analyzed entire tumor sections and reported antibody fluorescence as a function of distance from the nearest blood vessel (15). Lee et al. used a custom image analysis algorithm in the Image-Pro software to evaluate the impact of antibody dose and time after administration on the tumor penetration of trastuzumab and cetuximab (13). Here, we analyzed entire tumor sections from SKOV3 xenograft bearing mice administered trastuzumab or trastuzumab:1HE, using a combination of ImageJ and an in-house MATLAB algorithm. 1HE co-administration led to significant increases in the percent of the tumor section that stained positive for trastuzumab (26.52% (SD: 8.11) to 43.32% (SD: 11.42)) and the penetration distance of trastuzumab from vasculature (41.30 μm (SD: 6.70) to 58.24 μm (SD: 5.40). The values for the trastuzumab:1HE treated tumors are likely close to the upper limit. The maximum percent of the tumor area that can stain positive for trastuzumab is equal to the fraction of the tumor volume composed of antigen-expressing tumor cells. The tumor interstitial space has been reported to be between 20–60% of the total tumor volume (38); therefore, it is reasonable to assume the 43% positive staining area for the trastuzumab:1HE group is close to the cellular fraction of the tumor slice. The upper limit for trastuzumab's penetration distance is equal to the mean distance of all tumor pixels from the vasculature, which was 68.60 μm (SD: 15.65) and 64.54 μm (SD: 5.04) for the trastuzumab and trastuzumab:1HE groups. As a percent of the maximum penetration distance, the trastuzumab group was 61% while the trastuzumab:1HE group was 90%. In the present study, both functional and collapsed tumor vessels were stained; as a result, the true penetration limit is likely larger than the listed values, as only 10–50% of tumor vasculature is functional (39). Therefore, although 1HE significantly improved trastuzumab's penetration distance, the increase may be more dramatic than what the image analysis values suggests.

Antibody-drug conjugates can efficiently kill high antigen-expressing tumor cells, even when only a fraction of cellular antigens are occupied, due to the potency of the drug payload (40). Recently, it was predicted through mathematical modeling that T-DM1 with a lower drug-antibody ratio (DAR) would be more effective than a higher DAR due to the distribution benefit gained by spreading an equivalent mass of cytotoxic drug over a higher antibody dose (27). To validate this prediction, T-DM1 was given with free trastuzumab (effectively lowering the DAR) to mice bearing trastuzumab-resistant NCI-N87 xenografts (34). T-DM1 given alone was restricted to the peri-vasculature whereas T-DM1 given with carrier trastuzumab was homogenously distributed, leading to an improvement in the anti-tumor effect of T-DM1 (34). Singh et al. evaluated the trastuzumab / T-DM1 co-administration approach in multiple xenograft models and with multiple ratios of trastuzumab to T-DM1 (29). Trastuzumab co-administration with T-DM1 resulted in a synergistic interaction in mice bearing NCI-N87 xenografts, however, a less than additive effect was observed with trastuzumab co-administration in mice bearing the low HER2 expressing cell-line MDA-MB-453 (29). Ponte et al. applied the co-administration approach to an anti-folate receptor alpha antibody conjugated to DM4 or to a potent DNA alkylator in multiple xenograft models using multiple ratios of mAb:ADC (41). Enhancement of ADC efficacy was dependent on the tumor antigen expression, payload potency, and on the ratio

of unconjugated mAb:ADC (41). It is appreciated that using a carrier dose of unconjugated antibody to increase ADC efficacy is difficult to implement in the clinic (29,30,34,41). Patient-specific ratios of unconjugated antibody to ADC would be required due to patient-to-patient variability in HER2 receptor number, which can be difficult to quantify using current immunohistochemical scores. Relative to the approach of overcoming the BSB for ADC with co-administration of saturating doses of “naked” antibody, use of anti-idiotype inhibitors, such as 1HE, provides advantages. First, the time-course of inhibition of ADC binding is primarily dictated by the dissociation half-life of the anti-idiotype inhibitor and obviates the need for patient-specific optimization of mAb:ADC dosing ratios. Second, optimal dosing of naked antibody is highly dependent on tumor characteristics (size, vascularity) and, in situations where multiple tumors are present with varying size (e.g., large tumors and smaller metastases), it may be impossible to promote ADC distribution in large tumors without completely inhibiting ADC binding in small tumors (34). There is no similar concern relating to the use of anti-idiotype inhibitors to overcome the BSB, as the dissociation half-life of the inhibitor may be controlled to be far shorter than the plasma elimination half-life of the ADC.

The competitive inhibition approach is analogous to the probody approach, developed by CytomX, in which an antibody paratope is masked by a covalently linked peptide that contains a protease recognition sequence (42,43). Probodies improve the tumor selectivity of antibody therapy by limiting antibody binding to antigens that are expressed in healthy tissues through tumor-selective activation following protease cleavage of the masking agent in the tumor interstitial space (42,43). Probodies may facilitate improved tumor penetration, as masked antibodies can diffuse greater distances prior to protease-mediated unmasking; however, to our knowledge, enhanced tumor penetration of probodies relative to their parent mAb has not been thoroughly investigated. Additionally, in contrast to the enhanced efficacy that is observed with free mAb co-administration and our competitive inhibition strategy, the efficacy of probody-drug conjugates has been reported as being equivalent to the parent ADC (43). A key difference between the two strategies is the probody approach is dependent on tumor protease activity, whereas the competitive inhibition approach is independent of tumor physiology. Tumor protease expression is variable between patients and tumor types (44,45); therefore, the cleavage site of the masking sequence needs to be matched to the protease activity of the tumor (42). In a phase 1/2 clinical trial with the probody-drug conjugate CX-2009, the observed unmasked fraction of CX-2009 in a panel of patient tumor biopsies varied between 3%−53% (46). In contrast, the competitive inhibition strategy is primarily time-dependent and is not expected to vary significantly from patient-patient. Unlike probodies, co-administered competitive inhibitors are not expected to decrease the on-target, off-site binding of an antibody therapy as competitive inhibitor dissociation occurs at the same rate in healthy tissues as the tumor space. From a commercial standpoint, the probody strategy is attractive as it requires the development of a single entity. In-contrast, if the competitive inhibition approach is applied to a new antibody therapy, this would require the development of two entities (antibody/inhibitor). Therefore, the competitive inhibition strategy may best apply to already approved therapies (i.e. T-DM1) where the competitive inhibitor can be considered as an adjuvant. The commercial development of an anti-trastuzumab inhibitor is particularly attractive as there are two trastuzumab ADCs that are

FDA approved (ado-trastuzumab emtansine, trastuzumab deruxtecan) and a third in phase III clinical trials (trastuzumab duocarmazine) (47).

Although the effects observed following 1HE treatment are quite encouraging, we hypothesize that the results are far from optimal. Further improvements in tumor penetration of trastuzumab and efficacy of T-DM1 may be obtained through the optimization of 1HE affinity and dosing ratios. Mechanistic mathematical modeling may be applied to identify ideal inhibitor characteristics (e.g. optimizing the kinetics of inhibitor-antibody binding). As shown in our prior publications (32,48), our physiologically-based mechanistic mathematical models accurately predict the plasma and tissue disposition of antibodies, including non-linear dose-dependent mAb disposition in tumors and in human patients. The mechanistic nature of the models facilitates consideration of physiological variables (e.g., tumor size, antigen density, internalization kinetics) and drug characteristics (e.g., affinity, dissociation rate constants) and, thus, enables the in-silico exploration of relationships between inhibitor/mAb characteristics and metrics of interest (e.g., tumor disposition, tumor selectivity, time-averaged receptor occupancy).

The work shown here presents a new strategy to bypass the binding site barrier and improve antibody tumor distribution, without requirements of altering the native structure, affinity, or dosing protocol of the antibody. Transient competitive inhibition is a unique and elegant strategy that we believe can be easily adapted to any antibody therapeutic directed against solid tumor antigens. We have demonstrated competitive inhibition can improve trastuzumab distribution in solid tumors and improve T-DM1 efficacy in a mouse xenograft model.

Supplementary Material

Refer to Web version on PubMed Central for supplementary material.

Acknowledgements:

The authors would like to thank Mason McComb for his assistance with the tumor distribution algorithm. This work was funded by the National Institutes of Health/National Cancer Institute (Grants CA204192, CA246785).

Conflict of Interest Disclosure Statement: J.P.B. has served as a consultant to Genentech and Roche (on issues unrelated to the present work). In addition, J.P.B. serves as the Director of the University at Buffalo Center for Protein Therapeutics, which is supported by an industry consortium. Through the consortium, J.P.B. has received research support, for work unrelated to this report, from Abbvie, Amgen, CSL-Behring, Eli Lilly, Genentech, GSK, Janssen, Merck and Sanofi. During the course of this work, J.P.B. has received consulting fees from companies involved with the development of cancer therapies, including: Amgen, Eli Lilly, Merck, and Pfizer. J.P.B. and B.M.B. are inventors on a patent application that is related to this work (PCT/US2020/050159, pending).

REFERENCES

1. Kaplon H, Muralidharan M, Schneider Z, Reichert JM. Antibodies to watch in 2020. mAbs 2019:null–null
2. Jain RK, Baxter LT. Mechanisms of heterogeneous distribution of monoclonal antibodies and other macromolecules in tumors: significance of elevated interstitial pressure. Cancer Res 1988;48:7022–32 [PubMed: 3191477]
3. Jain RK. Physiological barriers to delivery of monoclonal antibodies and other macromolecules in tumors. Cancer Res 1990;50:814s–9s [PubMed: 2404582]

4. Cruz E, Kayser V. Monoclonal antibody therapy of solid tumors: clinical limitations and novel strategies to enhance treatment efficacy. Biologics 2019;13:33–51 [PubMed: 31118560]
5. Siegel RL, Miller KD, Jemal A. Cancer statistics, 2019. CA: A Cancer Journal for Clinicians 2019;69:7–34 [PubMed: 30620402]
6. Christiansen J, Rajasekaran AK. Biological impediments to monoclonal antibody-based cancer immunotherapy. Mol Cancer Ther 2004;3:1493–501 [PubMed: 15542788]
7. Eikenes L, Bruland OS, Brekken C, Davies Cde L. Collagenase increases the transcapillary pressure gradient and improves the uptake and distribution of monoclonal antibodies in human osteosarcoma xenografts. Cancer Res 2004;64:4768–73 [PubMed: 15256445]
8. Singha NC, Nekoroski T, Zhao C, Symons R, Jiang P, Frost GI, et al. Tumor-Associated Hyaluronan Limits Efficacy of Monoclonal Antibody Therapy. Molecular Cancer Therapeutics 2015;14:523 [PubMed: 25512619]
9. Beyer I, Li Z, Persson J, Liu Y, van Rensburg R, Yumul R, et al. Controlled extracellular matrix degradation in breast cancer tumors improves therapy by trastuzumab. Mol Ther 2011;19:479–89 [PubMed: 21081901]
10. Sugahara KN, Teesalu T, Karmali PP, Kotamraju VR, Agemy L, Greenwald DR, et al. Coadministration of a tumor-penetrating peptide enhances the efficacy of cancer drugs. Science 2010;328:1031–5 [PubMed: 20378772]
11. Shin TH, Sung ES, Kim YJ, Kim KS, Kim SH, Kim SK, et al. Enhancement of the tumor penetration of monoclonal antibody by fusion of a neuropilin-targeting peptide improves the antitumor efficacy. Mol Cancer Ther 2014;13:651–61 [PubMed: 24435448]
12. Hu P, Hornick JL, Glasky MS, Yun A, Milkie MN, Khawli LA, et al. A chimeric Lym-1/interleukin 2 fusion protein for increasing tumor vascular permeability and enhancing antibody uptake. Cancer Res 1996;56:4998–5004 [PubMed: 8895756]
13. Lee CM, Tannock IF. The distribution of the therapeutic monoclonal antibodies cetuximab and trastuzumab within solid tumors. BMC Cancer 2010;10:255 [PubMed: 20525277]
14. Rudnick SI, Adams GP. Affinity and avidity in antibody-based tumor targeting. Cancer Biother Radiopharm 2009;24:155–61 [PubMed: 19409036]
15. Rhoden JJ, Wittrup KD. Dose dependence of intratumoral perivascular distribution of monoclonal antibodies. J Pharm Sci 2012;101:860–7 [PubMed: 22057714]
16. Juweid M, Neumann R, Paik C, Perez-Bacete MJ, Sato J, van Osdol W, et al. Micropharmacology of Monoclonal Antibodies in Solid Tumors: Direct Experimental Evidence for a Binding Site Barrier. Cancer Research 1992;52:5144–53 [PubMed: 1327501]
17. Adams GP, Schier R, McCall AM, Simmons HH, Horak EM, Alpaugh RK, et al. High affinity restricts the localization and tumor penetration of single-chain fv antibody molecules. Cancer Res 2001;61:4750–5 [PubMed: 11406547]
18. Rudnick SI, Lou J, Shaller CC, Tang Y, Klein-Szanto AJ, Weiner LM, et al. Influence of affinity and antigen internalization on the uptake and penetration of Anti-HER2 antibodies in solid tumors. Cancer Res 2011;71:2250–9 [PubMed: 21406401]
19. Fujimori K, Covell DG, Fletcher JE, Weinstein JN. A modeling analysis of monoclonal antibody percolation through tumors: a binding-site barrier. J Nucl Med 1990;31:1191–8 [PubMed: 2362198]
20. Schmidt MM, Wittrup KD. A modeling analysis of the effects of molecular size and binding affinity on tumor targeting. Mol Cancer Ther 2009;8:2861–71 [PubMed: 19825804]
21. Adams GP, Schier R, Marshall K, Wolf EJ, McCall AM, Marks JD, et al. Increased affinity leads to improved selective tumor delivery of single-chain Fv antibodies. Cancer Res 1998;58:485–90 [PubMed: 9458094]
22. Thurber GM, Schmidt MM, Wittrup KD. Antibody tumor penetration: transport opposed by systemic and antigen-mediated clearance. Adv Drug Deliv Rev 2008;60:1421–34 [PubMed: 18541331]
23. Thurber GM, Wittrup KD. Quantitative spatiotemporal analysis of antibody fragment diffusion and endocytic consumption in tumor spheroids. Cancer Res 2008;68:3334–41 [PubMed: 18451160]
24. Thurber GM, Zajic SC, Wittrup KD. Theoretic Criteria for Antibody Penetration into Solid Tumors and Micrometastases. Journal of Nuclear Medicine 2007;48:995–9 [PubMed: 17504872]

25. Debie P, Lafont C, Defrise M, Hansen I, van Willigen DM, van Leeuwen FWB, et al. Size and affinity kinetics of nanobodies influence targeting and penetration of solid tumours. J Control Release 2020;317:34–42 [PubMed: 31734445]
26. Cilliers C, Guo H, Liao J, Christodolu N, Thurber GM. Multiscale Modeling of Antibody-Drug Conjugates: Connecting Tissue and Cellular Distribution to Whole Animal Pharmacokinetics and Potential Implications for Efficacy. AAPS J 2016;18:1117–30 [PubMed: 27287046]
27. Khera E, Cilliers C, Bhatnagar S, Thurber GM. Computational transport analysis of antibody-drug conjugate bystander effects and payload tumoral distribution: implications for therapy. Molecular Systems Design & Engineering 2018
28. Cilliers C, Menezes B, Nessler I, Linderman J, Thurber GM. Improved Tumor Penetration and Single-Cell Targeting of Antibody–Drug Conjugates Increases Anticancer Efficacy and Host Survival. Cancer Research 2018;78:758–68 [PubMed: 29217763]
29. Singh AP, Guo L, Verma A, Wong GG-L, Thurber GM, Shah DK. Antibody Coadministration as a Strategy to Overcome Binding-Site Barrier for ADCs: a Quantitative Investigation. The AAPS Journal 2020;22:28 [PubMed: 31938899]
30. Menezes B, Cilliers C, Wessler T, Thurber GM, Linderman JJ. An Agent-Based Systems Pharmacology Model of the Antibody-Drug Conjugate Kadcyla to Predict Efficacy of Different Dosing Regimens. The AAPS Journal 2020;22:29 [PubMed: 31942650]
31. Alvarez-Rueda N, Ladjemi MZ, Béhar G, Corgnac S, Pugnière M, Roquet F, et al. A llama single domain anti-idiotypic antibody mimicking HER2 as a vaccine: Immunogenicity and efficacy. Vaccine 2009;27:4826–33 [PubMed: 19523913]
32. Garg A, Balthasar JP. Physiologically-based pharmacokinetic (PBPK) model to predict IgG tissue kinetics in wild-type and FcRn-knockout mice. J Pharmacokinet Pharmacodyn 2007;34:687–709 [PubMed: 17636457]
33. Abuqayyas L, Balthasar JP. Pharmacokinetic mAb-mAb interaction: anti-VEGF mAb decreases the distribution of anti-CEA mAb into colorectal tumor xenografts. AAPS J 2012;14:445–55 [PubMed: 22528507]
34. Cilliers C, Menezes B, Nessler I, Linderman J, Thurber GM. Improved Tumor Penetration and Single-Cell Targeting of Antibody-Drug Conjugates Increases Anticancer Efficacy and Host Survival. Cancer Res 2018;78:758–68 [PubMed: 29217763]
35. Abuqayyas L. Evaluation of The Mechanistic Determinants for IgG Exposure in Tissues: University at Buffalo; 2012.
36. Awuah P, Bera TK, Folivi M, Chertov O, Pastan I. Reduced Shedding of Surface Mesothelin Improves Efficacy of Mesothelin-Targeting Recombinant Immunotoxins. Mol Cancer Ther 2016;15:1648–55 [PubMed: 27196771]
37. Pak Y, Zhang Y, Pastan I, Lee B. Antigen shedding may improve efficiencies for delivery of antibody-based anticancer agents in solid tumors. Cancer Res 2012;72:3143–52 [PubMed: 22562466]
38. Jain RK. Transport of Molecules in the Tumor Interstitium: A Review. Cancer Research 1987;47:3039–51 [PubMed: 3555767]
39. Nia HT, Liu H, Seano G, Datta M, Jones D, Rahbari N, et al. Solid stress and elastic energy as measures of tumour mechanopathology. Nat Biomed Eng 2016;1
40. Govindan SV, Sharkey RM, Goldenberg DM. Prospects and progress of antibody-drug conjugates in solid tumor therapies. Expert Opin Biol Ther 2016;16:883–93 [PubMed: 27045979]
41. Ponte JF, Lanieri L, Khera E, Laleau R, Ab O, Espelin C, et al. Antibody Co-Administration Can Improve Systemic and Local Distribution of Antibody-Drug Conjugates to Increase In Vivo Efficacy. Mol Cancer Ther 2021;20:203–12 [PubMed: 33177153]
42. Kavanaugh WM. Antibody prodrugs for cancer. Expert Opin Biol Ther 2020;20:163–71 [PubMed: 31779489]
43. Lin J, Sagert J. Targeting Drug Conjugates to the Tumor Microenvironment: Probody Drug Conjugates. In: Damelin M, editor. Innovations for Next-Generation Antibody-Drug Conjugates. Cham: Springer International Publishing; 2018. p 281–98.

44. Vasiljeva O, Menendez E, Nguyen M, Craik CS, Michael Kavanaugh W. Monitoring protease activity in biological tissues using antibody prodrugs as sensing probes. Scientific Reports 2020;10:5894 [PubMed: 32246002]

45. LeBeau AM, Sevillano N, Markham K, Winter MB, Murphy ST, Hostetter DR, et al. Imaging Active Urokinase Plasminogen Activator in Prostate Cancer. Cancer Research 2015;75:1225–35 [PubMed: 25672980]

46. Liu J. Intratumoral Activation and Phase 1/2 Clinical Activity of Praluzatamab Ravtansine (CX-2009), a Probody® Drug Conjugate (PDC) Targeting CD166 (PS11–07). San Antonio Breast Cancer Symposium. San Antonio, TX: CytomX Therapeutics, Inc.; 2020.

47. Rinnerthaler G, Gampenrieder SP, Greil R. HER2 Directed Antibody-Drug-Conjugates beyond T-DM1 in Breast Cancer. Int J Mol Sci 2019;20

48. Glassman PM, Balthasar JP. Physiologically-based pharmacokinetic modeling to predict the clinical pharmacokinetics of monoclonal antibodies. J Pharmacokinet Pharmacodyn 2016;43:427–46 [PubMed: 27377311]

Significance:

This study describes the development of a transient competitive inhibition strategy that enhances the tumor penetration and efficacy of anti-cancer antibodies.

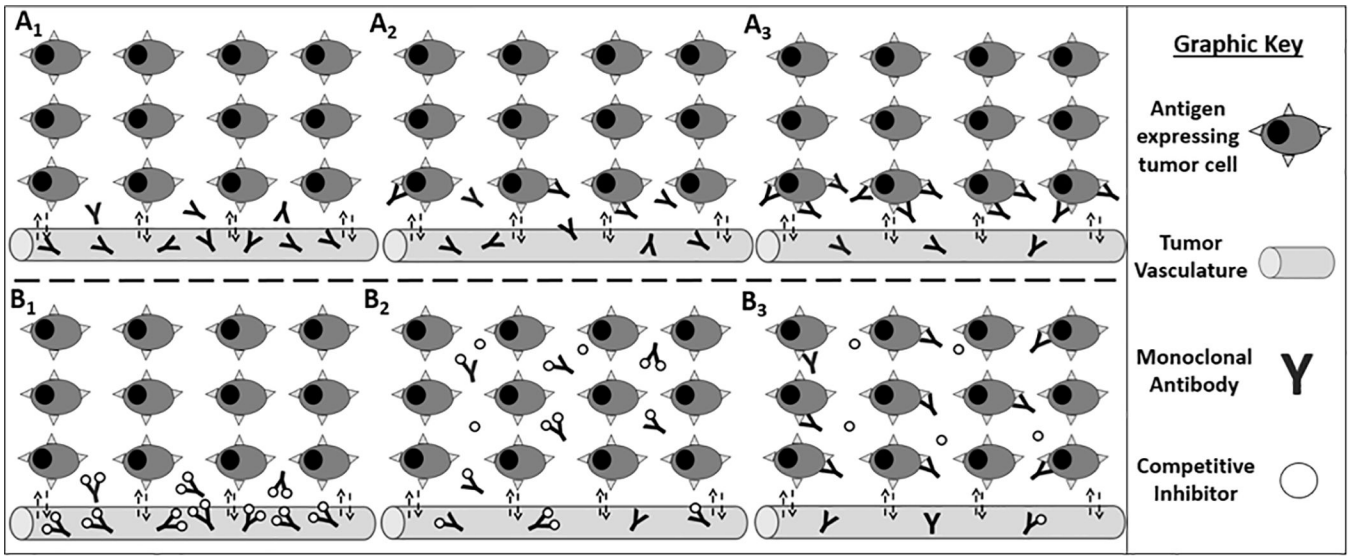

Figure 1: Bypassing the binding site barrier: a graphic representation of the competitive inhibition strategy

The top panels represent the binding site barrier, with mAbs that extravasate into the tumor (A1) successfully binding antigen-expressing cells in the perivascular region (A2), with tumor cells distant from vasculature remaining untargeted (A3). The bottom panels represent the competitive inhibition strategy with the mAb-inhibitor complex extravasating into the tumor (B1) and diffusing throughout the interstitial space (B2). Over time the mAb-inhibitor complex dissociates with free antibody binding antigen-expressing cells at the point of dissociation, improving tumor cell targeting (B3).

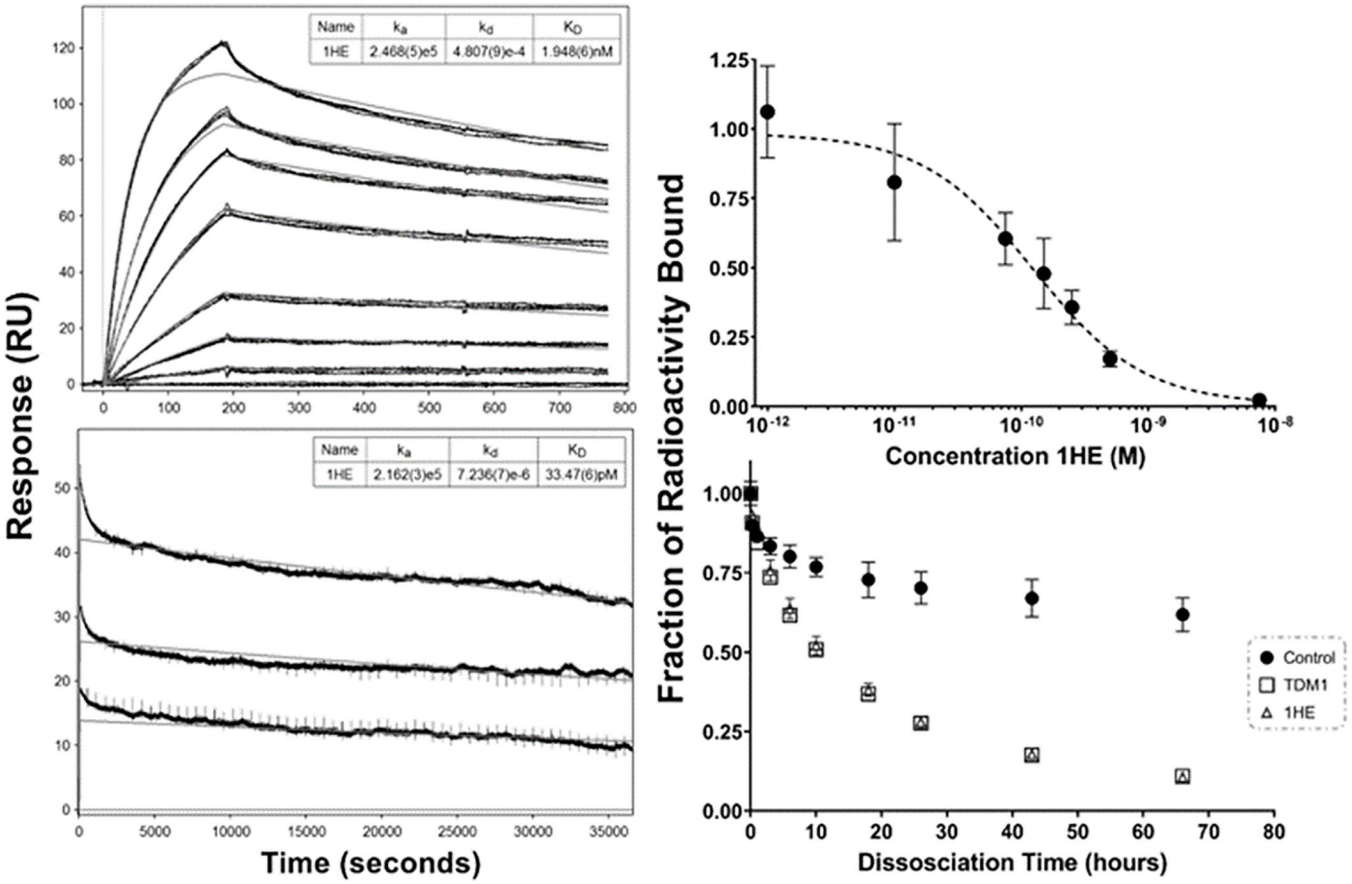

Figure 2: 1HE-trastuzumab binding characterization

The initial SPR evaluation of 1HE-trastuzumab binding with a ten-minute dissociation is shown in the top left panel. A second SPR run with a 10-hour dissociation time frame is shown in the bottom left panel. Model fits for the association rate constant (ka), dissociation rate constant (kd), and equilibrium dissociation rate constant (KD) are shown in the top right for each sensorgram with standard deviation for each parameter provided in brackets. Similar association rate constants were observed between runs while the best fit dissociation rate constant was 4.8×10^{-4} sec^{-1} for the 10-minute dissociation and 7.2×10^{-6} sec^{-1} for the 10-hour dissociation. Shown in the top right panel is the competitive cell inhibition assay to assess the impact of 1HE on trastuzumab-HER2 binding, shown is the ratio of ^{125}I-trastuzumab bound to SKOV3 cells (as measured by cell-associated radioactivity) when incubated with 1HE in comparison to a ^{125}I-trastuzumab only control. 1HE inhibited trastuzumab-HER2 binding with an IC50 of 124 pM. The dissociation of 125I-1HE from trastuzumab immobilized magnetic beads is shown in the bottom right panel. ^{125}I-1HE bound beads were incubated with a 0.1% BSA-PBS control or with 1 μM ado-trastuzumab emtansine (T-DM1), or 1 μM cold-1HE in 0.1% BSA-PBS to prevent rebinding. At the indicated time-points, the supernatant was removed, fresh buffer-solution added, and bound radioactivity assessed. The addition of cold-1HE or free trastuzumab emtansine (T-DM1) led to overlaying dissociation curves, whereas the dissociation rate in blank buffer was significantly slower due to ^{125}I-1HE rebinding trastuzumab-beads. Individual points represent the mean of triplicate samples with standard deviation error bars.

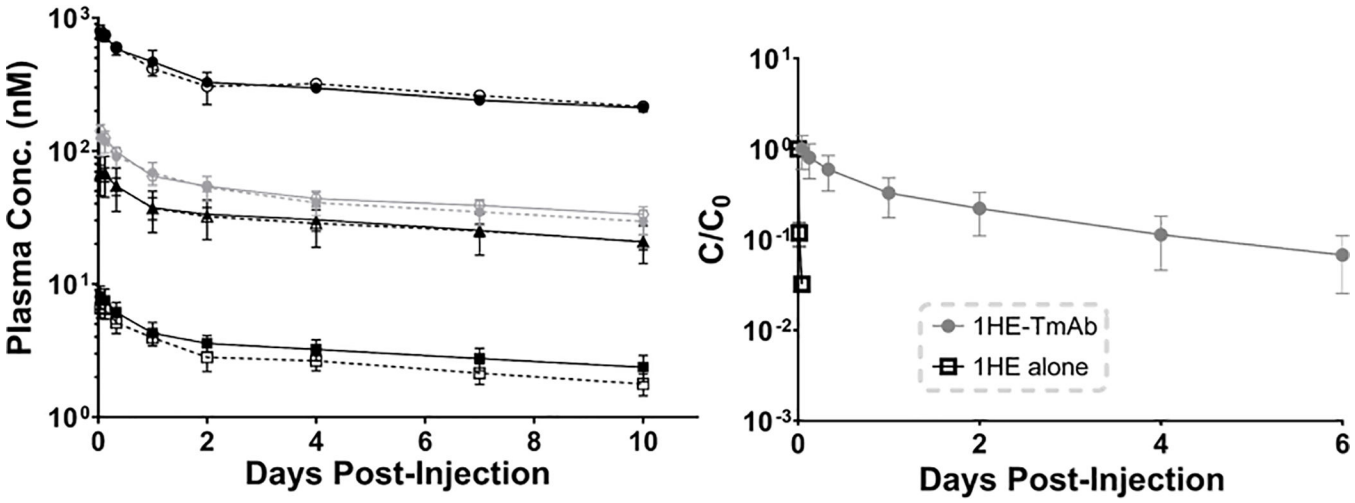

Figure 3: Trastuzumab plasma pharmacokinetics with and without 1HE co-administration

(Left) Plasma time profiles for trastuzumab (black) or T-DM1 (gray) administered alone (closed symbols) or in combination with 1HE (open symbols) at a dose of 10 mg/kg (circles), 1.8 mg/kg (diamonds), 1 mg/kg (triangles), and 0.1 mg/kg (squares). (Right) Plasma time profiles for 1HE administered at a 1 mg/kg dose alone (black open squares) or 1HE administered with 1 mg/kg trastuzumab (gray circles) is shown. 1HE administered alone is rapidly eliminated, consistent with expectations for a ~15 kDa protein, while 1HE co-administered with trastuzumab has an increased plasma half-life.

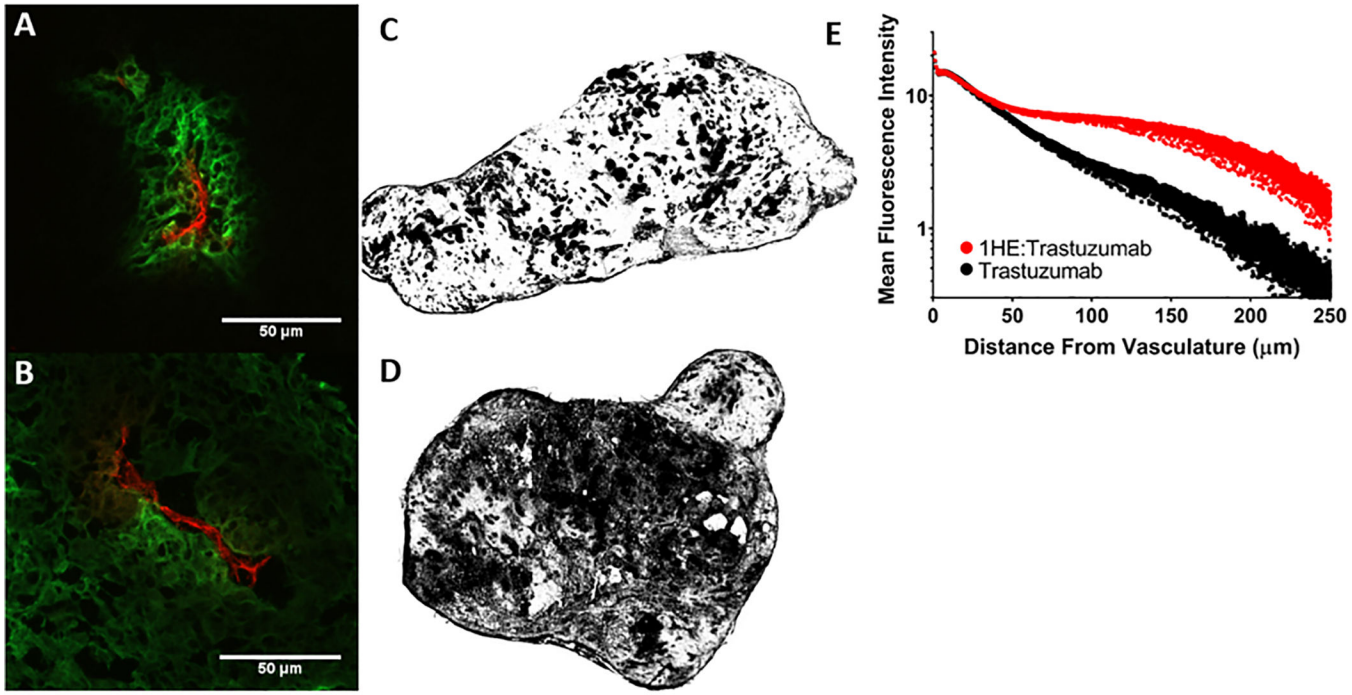

Figure 4: Impact of 1HE co-administration on trastuzumab distribution in SK-OV3 xenografts

(A) Trastuzumab administered alone (green) is restricted around vasculature (red) whereas (B) 1HE co-administration increased trastuzumab tumor penetration as indicated by the diffuse staining from the point of extravasation. Whole tumor sections of trastuzumab and trastuzumab:1HE are shown in C and D respectively, images were converted to black and white with regions of trastuzumab positive fluorescent staining two-fold greater than background appearing in black. In comparison to tumors treated with trastuzumab alone. 1HE co-administration dramatically increased the fraction of the tumor that stained positive for trastuzumab. Trastuzumab associated fluorescence staining (MFI) as a function of distance from the nearest blood vessel is shown with and without 1HE co-administration. Individual points represent the mean of all pixels at a given distance from the vasculature. Similar fluorescence intensity is observed for trastuzumab administered alone and with 1HE up to 30 μm from the vasculature. Starting at 30 μm the trastuzumab:1HE group has greater staining intensity which extends up to 250 μm from the vasculature.

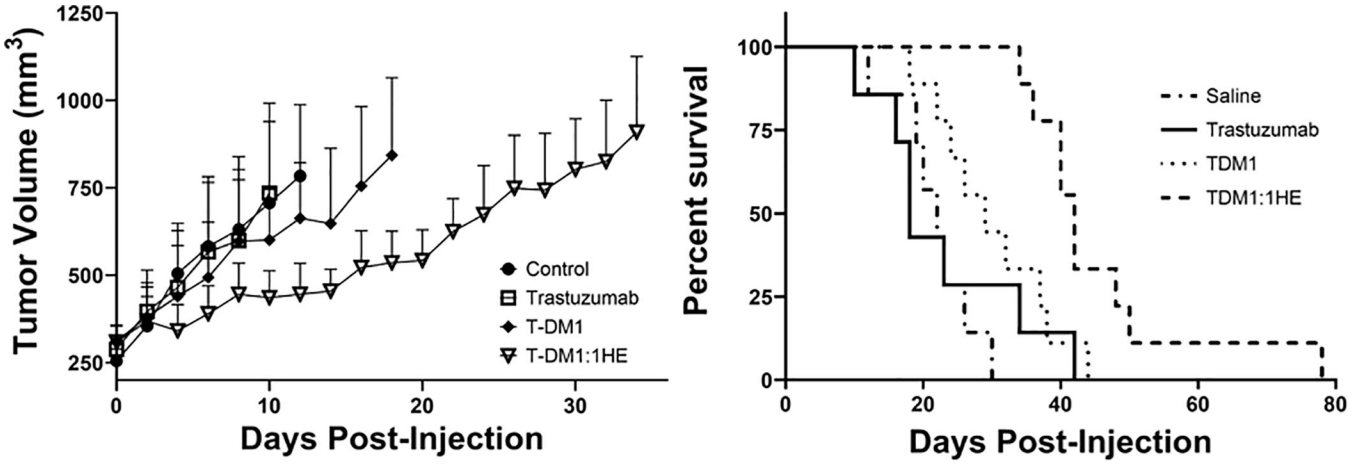

Figure 5: Impact of 1HE co-administration on T-DM1 efficacy in NCI-N87 xenograft bearing mice

(Left) Tumor growth curves for each dose group with curves ending at the first death event (tumor volume greater than 1200 mm^3). Tumor volume data represents the group mean with standard deviation error bars. (Right) Survival curves are shown for each group with statistical significance in survival using the log-rank test with significance set at $p \leq 0.008$ using Bonferonnis correction for multiple comparisons. Trastuzumab did not significantly extend lifespan in comparison to the control group (p=0.68). T-DM1 alone did not significantly improve survival from the saline group (p=0.033) or the trastuzumab group (p=0.27). T-DM1 co-administered with 1HE had a significant increase in survival from T-DM1 alone (p=0.005) and both the trastuzumab (p=0.004) and saline groups (p<0.0001).

Table 1:

Trastuzumab/T-DM1 Plasma AUCs with and without 1HE

Dose Group	AUClast (day×nM)	AUClast with 1HE (day×nM)	P-value
Trastuzumab 0.1 mg/kg	33.18 ±5.071	26.83 ±3.96	0.06
Trastuzumab 1 mg/kg	302.9 ±37.45	295.6 ±98.89	0.88
T-DM1 1.8 mg/kg	479.7 ±40.08	450.3 ±71.31	0.44
Trastuzumab 10 mg/kg	3077 ±121.2	3133 ±239.7	0.66

Table 2:

Quantitative Fluorescent Image Analysis

Parameter	Trastuzumab	Trastuzumab:1HE	p-value
Positive Trastuzumab Area (SD)	26.52% (±8.11%)	43.32% (±11.42%)	0.0024
Mean Trastuzumab Fluorescence (SD)	13 MFI (±3)	15 MFI (±4)	0.25
Mean Trastuzumab Fluorescence for pixels above 10 (SD)	34 MFI (±5)	27 MFI (±3)	0.0034
Penetration Distance Limit (SD)	68.60 μm (±15.65 μm)	64.54 μm (±5.04 μm)	0.47
Grayscale Penetration Distance (SD)	39.38 μm (±5.89 μm)	51.52 μm (±5.15 μm)	0.0003
Percent of Grayscale to Limit (SD)	58.39% (±5.70%)	79.97% (±7.00%)	<0.0001
Threshold Penetration Distance (SD)	41.30 μm (±6.70 μm)	58.24 μm (±5.40 μm)	<0.0001
Percent of Threshold to Limit (SD)	61.15% (±6.26%)	90.34% (±6.02%)	<0.0001